

# Temporal evolution and rigidity dependence of the solar modulation lag of Galactic cosmic rays

Nicola Tomassetti, Bruna Bertucci, Emanuele Fiandrini  
*Dipartimento di Fisica e Geologia, Università degli Studi di Perugia, Italy*

When traveling in the heliosphere, Galactic cosmic rays (CRs) are subjected to the solar modulation effect, a quasiperiodical change of their intensity caused by the 11-year cycle of solar activity. Here we investigate the association of solar activity and cosmic radiation over five solar cycles, from 1965 to 2020, using a collection of multichannel data from neutron monitors, space missions, and solar observatories. In particular, we focus on the time lag between the monthly sunspot number and the CR flux variations. We show that the modulation lag is subjected to a 22-year periodical variation, ranging from about 2 to 14 months and following the polarity cycle of the Sun's magnetic field. We also show that the lag is remarkably decreasing with increasing energy of the CR particles. These results reflect the interplay of basic physics phenomena that cause the CR modulation effect: the drift motion of charged particles in the interplanetary magnetic field, the latitudinal dependence of the solar wind, the energy dependence of their residence time in the heliosphere. Based on this interpretation, we end up with a global effective formula for the modulation lag and testable predictions for the flux evolution of cosmic particles and antiparticles over the solar cycle.

## I. INTRODUCTION

When traveling inside the heliosphere, Galactic cosmic rays (CRs) interact with magnetic fields and solar wind disturbances, which cause variations in their intensity and energy spectrum. This phenomenon is known as *solar modulation* of CRs and it is crucial for the investigation of the origin of cosmic particles and antiparticles [1]. Understanding CR modulation is also important for assessing the radiation dose and risk in manned space missions [2]. In this respect, there are strong efforts aimed at predicting the evolution of the CR intensity near-Earth or in the interplanetary space [3]. An important feature of solar modulation is its connection with the 11-year cycle of solar activity. The monthly *sunspot number* (SSN), the main indicator of solar cycle, is known to be anticorrelated with the long-term variations of the CR flux [4–6]. During periods of solar cycle minimum, the flux of Galactic CRs in the inner heliosphere is more intense. During periods of solar cycle maximum, CRs are shielded more effectively by the Sun. Other proxies for solar activity include the intensity of the solar magnetic field  $B_0$ , its open magnetic flux, or the tilt angle of the heliospheric current sheet.

Solar activity is constantly monitored by ground based observatories or space probes. The time dependence of the CR flux is measured by several experiments. Direct measurements of particle- and energy-resolved CR flux have been done in space by long-running experiments such as the MED instrument on IMP-8 (since 1972 to 2000 [7]), the HET telescopes on the Voyager probes (1979-present [8]), the spectrometers CRIS on ACE (1997-present [9]), EPHIN on SOHO (1995-present [10]). Recent measurements include the spectrometers PAMELA on the Resurs-DK1 satellite (2006-2016 [11, 12]) and AMS on the International Space Station (2011-present [13, 14]). Indirect measurements of the CR time dependence are performed continuously, since

the 1950s, by neutron monitors (NMs) [15]. NMs show excellent time resolution and exposure, but they have no particle or energy resolution capabilities.

To understand the dynamics of CR modulation and its association with solar activity, it is important to study the *time lag* between the two phenomena. Several studies reported a lag of few months between the monthly SSN and the corresponding variations in the NM rates [16–24]. Using direct CR measurements from space experiments, a lag of  $8.1 \pm 0.1$  months was reported for Solar Cycle 23 [25]. Similar lags were also observed using different proxies such as tilt angle or magnetic field [26]. Such a lag in CR modulation is usually interpreted in terms of the plasma dynamics [27–29]. In fact, the time dependence of CRs near-Earth is linked to their transport through the expanding heliosphere. To first approximation, the lag between CRs and solar activity reflects the time spent by the heliospheric plasma to travel from the Sun to the whole modulation region, which is of the order of one year. Other interpretations of the lag include a delayed response of the CRs to changes in the background plasma, or delayed formation of the solar magnetic field with respect to sunspots [5, 30, 31]. On the lag values reported in different analysis there is no clear consensus, as they range from 0 to 18 months depending on epochs, cycles, NM stations, or indicators [16, 22, 23]. Previous studies reported a remarkable odd-even dependence of the lag in terms of cycle number. This effect may be ascribed to the role of drift in the heliospheric modulation process [17].

In this paper, we investigate the delayed relationship between solar activity and CR flux over five solar cycles between 1965 and 2020, *i.e.*, from Cycles 20 to 25. In Sec. II, we present the theoretical framework to analyze the long-term CR modulation using NM and spacecraft data. In Sec. III, we present the main results of our correlation analysis. In particular, we present a reconstruction of the CR modulation lag over the solar cycle. We show that the lag is subjected to a quasiperiodical evolution,

following the 22-year cycle of magnetic polarity, while its average value is found to decrease with the increasing rigidity (or energy) of the cosmic particles. Based on these findings, we also provide an effective formula to describe the temporal evolution and the rigidity dependence of the CR modulation lag. This constitute an essential input for developing predictive models of CR modulation [32–37]. In Sec. IV A, we discuss the astrophysical interpretation of our findings. We argue that the two features can be interpreted as signatures of charge-sign dependent drift and energy-dependent diffusion of CRs in the heliosphere, respectively. This may offer a new way to investigate basic plasma astrophysics processes in the heliosphere. Based on this interpretation, we also provide testable predictions using CR flux measurements of particles and antiparticles.

## II. CALCULATIONS

Our work is based on three main sets of data organized in forms of time series: direct measurements of CR fluxes performed in space, counting rates of secondary particles recorded by NMs, and the monthly SSN recorded in solar observatories. In this section, we present our calculation framework. First, we briefly outline our calculations for the local interstellar spectra (LIS) of the main CR species. Then, we present the solar modulation calculations used to describe the temporal dependence of the top-of-atmosphere (TOA) fluxes. Finally, we present the modeling of the counting rate of ground NM detectors.

### A. Modeling the LIS fluxes

In this work, LIS fluxes are used as a mere input for the heliospheric modulation calculations. The investigation of the CR propagation in interstellar space is beyond the scope of this work. Nonetheless, we opted for fully numerical calculations that incorporates the essential physics of interstellar CR transport. Such an approach allows for a robust estimation of the LIS model uncertainties, that are considerable in the GeV energy region where no direct data are available [39, 40]. The relevant LISs for this work are the most abundant species such as CR proton ( $\sim 90\%$ ) and helium nuclei ( $\sim 9\%$ ). They are predominantly of primary origin, *i.e.*, accelerated by nonthermal processes in supernova shockwaves or stellar winds. Other species such as C-N-O nuclei or rarer elements are of minor relevance. To constrain the Galactic propagation parameters, however, calculations of secondary species such as lithium or boron are of fundamental importance. In our calculations, we implemented a *two-halo model* of CR propagation in the Galaxy [41, 42]. In this model, the transport of CRs in the ISM is described by spatial dependent diffusion of CRs in a two-zone magnetic turbulence, along with their interactions with the gas in the galactic disk. The acceler-

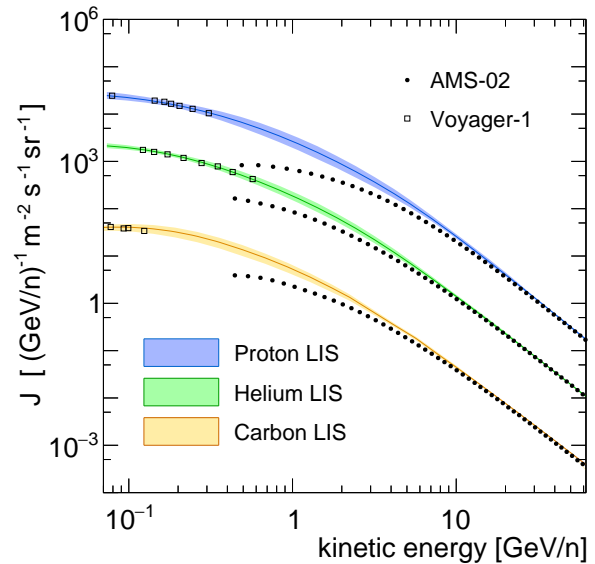


FIG. 1. LIS calculations for CR proton, helium, and carbon fluxes in comparison with direct measurements from AMS in the ISS and Voyager-1 in interstellar space [8, 43, 44].

ation of primary CRs is described by rigidity-dependent source functions of the type  $S_p \propto (R/GV)^{-\nu}$ , with index  $\nu = 2.28 \pm 0.12$  for  $Z = 1$  and index  $\nu = 2.35 \pm 0.13$  for all  $Z > 1$  nuclei. The production of secondary particles is calculated using source functions of the type  $S_s = \sum_h \Gamma_{h \rightarrow s}^{\text{sp}} N_h$ , which describe the  $h \rightarrow s$  fragmentation of  $h$ -type species of density  $N_h$  into  $s$ -type nuclei at rate  $\Gamma_{h \rightarrow s}$ . In this description, the physics processes of acceleration, nuclear fragmentation and ionization losses occur in the Galactic disk, *i.e.*, where the sources and the matter are placed. The diffusive transport of CRs takes place in an extended halo of vertical size  $L$ . The CR diffusion coefficient in the Galaxy is expressed as  $D \equiv \beta D_0 (R/GV)^{\delta_i/\delta_o}$ , where we assume two diffusion regimes: a shallow diffusion for the near-disk region with index  $\delta_i$  within distance  $z \leq \xi L$  from the disk, and a faster diffusion in the extended halo with index  $\delta_o \equiv \delta_i + \Delta$ . Based on our fits, we adopt  $\delta_i = 0.18 \pm 0.05$  and  $D_0/L = 0.01 \pm 0.002$  kpc/Myr,  $\Delta = 0.55 \pm 0.11$ , and  $\xi = 0.12 \pm 0.03$ . Diffusive reacceleration is also accounted, although our propagation scenario favors models with no reacceleration. The propagation calculations are made for all nuclear species in CR from  $Z = 1$  to  $Z = 26$ . All LIS fluxes are evaluated at the position of the Solar System, in cylindrical coordinates  $z_\odot \cong 0$  of height and  $r_\odot \cong 8.3$  kpc of galactocentric radius. The calculations are described in details in our past works [39, 40, 42]. The key model parameters are constrained using LIS data from Voyager-1 [8], high-energy measurements on primary nuclei (p-He-C-O) from AMS [43, 44], and secondary to primary ratios [14, 45]. The calculated LIS fluxes are illustrated in Fig. 1 in comparison with the data for the three most abundant CR species.

## B. Modeling the TOA fluxes

We now present the calculations for the time-dependent modulation of CRs near Earth. The solar modulation effect is determined by basic transport processes inside the heliosphere. To compute the CR fluxes at a given epoch and in a given location in the heliosphere, one has to solve the Parker's equation of CR transport. In its general form, the equation accounts for diffusion in the small-scale irregularities of the interplanetary magnetic field, gradient and curvature drift across its large-scale components, convection with the solar wind and adiabatic energy losses [1]. Here we employ the simple *force field* (FF) solar modulation model. The FF model is a simplified solution of the Parker's equation for a spherically symmetric wind and an isotropic diffusion coefficient. The model provides a simple one-to-one correspondence between TOA and LIS fluxes in terms of a lower shift in kinetic energy of the CR density [47, 48]. For a CR nucleus of mass  $M$ , atomic number  $Z$  and mass number  $A$ , the TOA flux  $J$  is related to its interstellar value  $J^{\text{IS}}$  by the relation:

$$J(E) = \frac{E(E + 2m_p)}{(E + \Phi)(E + \Phi + 2m_p)} \times J^{\text{IS}}(E + \Phi), \quad (1)$$

where  $E \equiv T/A$  is the kinetic energy per nucleon, and  $m_p \cong M/A$  is the nucleon mass. The sum  $E + \Phi$  is the kinetic energy per nucleon of CRs outside the heliosphere. The parameter  $\Phi \equiv (eZ/A)\phi$  represents the mean kinetic energy loss of CRs in the heliosphere, and  $\phi$  is the so-called *modulation potential*. The CR modulation of all CR nuclei is then described by a unique parameter,  $\phi$ , which has the dimension of an electric potential or a rigidity. The modulation potential is related to physical quantities such as diffusion coefficient  $K$ , solar wind speed  $V$ , and heliospheric boundaries  $r_{\text{hp}}$  as:

$$\phi = \int_{r_0}^{r_{\text{hp}}} \frac{V(r)}{3K(r)} dr, \quad (2)$$

where  $r_0 = 1 \text{ AU}$  is our location. With a quasi-stationary approach, the long-term variations of the CR fluxes can be expressed in terms of a time-dependent modulation parameter  $\phi = \phi(t)$ . Several strategies have been developed for the reconstruction of the modulation level  $\phi(t)$  at different epochs [6, 49]. The FF model suffers from severe limitations [48, 50]. It does not capture physical mechanisms such as drift or anisotropic diffusion, that require more advanced modeling [51–54]. Another problem is the applicability of the quasi-steady-state approximation [40]. We emphasize, however, that for the purpose of this work the  $\phi$  parameter is regarded a mere proxy for the time variations of the CR modulation. Thus, it is not regarded as a physical quantity representing the conditions of the heliospheric plasma. As we will see, the convenience of the FF model is to express the time-dependent response of different detectors into comparable time series of a unique parameter.

## C. Modeling the NM response

We now present a parametric description of the NM rates and their link with the time-dependent CR fluxes. The rate  $\mathcal{R}_{\text{NM}}^d$  of a NM detector  $d$  at given epoch  $t$  after correction for the barometric pressure is given by [6, 55, 56]:

$$\mathcal{R}^d(t) = \sum_{j=\text{CRs}} \int_0^\infty dE \cdot \mathcal{H}_j^d(E) \cdot \mathcal{Y}_j^d(E) \cdot J_j(t, E). \quad (3)$$

The sum is extended to all contributing CR species, where the solar modulated flux of the  $j$ -th species is  $J_j(t, E)$ . In practice we consider only proton and helium. Heavier nuclei such as carbon or oxygen contribute to a  $\sim 1\%$  of the NM rate, and with a very similar temporal dependence. The  $\mathcal{Y}_j^d(E)$  function is the so-called yield function, measured in  $m^2 sr$ . It captures the energy-dependent response of a NM to  $j$ th-type CRs at unit intensity. It includes the physics of hadronic showering in the atmosphere, the detection efficiency of the instrument, its absolute normalization, its dependence on altitude [57]. In this work, to compute the NM yield, we implemented the parametric model of Maurin et al. [49] (see Sec. 4.2). The factor  $\mathcal{H}^d$  in Eq. 3 is a *transmission function*. It accounts for the geomagnetic field modulation of CRs. We model it as a smoothed Heavyside function of rigidity [58]:

$$\mathcal{H}_j^d(E) = \frac{1}{1 + [R_j(E)/R_C^d]^{-s}}, \quad (4)$$

where  $R_C^d$  is the geomagnetic cutoff rigidity of a given NMs station and  $s = 12$  sets the sharpness of the transition. The transmission function is assumed constant in time, although the parameter  $R_C^d$  is subjected to slow secular variations [59]. The transmission function is also particle independent when expressed as function of rigidity,  $\mathcal{H}(R)$ . In Eq. 4, the  $j$ -dependence arises from the relation between rigidity and kinetic energy per nucleon,

$$R_j = (A_j/Z_j) [E^2 + 2m_p E]^{1/2}, \quad (5)$$

which contains the mass/charge ratio of the  $j$ -th specie. We also note that, due to geomagnetic transmission, the energy integration of Eq. 3 contributes for  $E \gtrsim E_C^j$ , *i.e.*, above the energy corresponding to the local cutoff  $R_C$ :

$$E_C^j = \left[ R_C^2 (Z_j/A_j)^2 + m_p^2 \right]^{1/2} - m_p. \quad (6)$$

For this reason, other authors set a lower limit  $E_C$  in the integration of the NM rate, in place of using the  $H$  function [49, 55, 56]. Once the NM response is fully specified, variations of the NM rates  $\mathcal{R}_{\text{NM}}^d(t)$  can be directly related to the time dependence of the TOA CR fluxes  $J_j = J_j(t, E)$ . Moreover, as seen in Sec. II B, the modulated fluxes can be related to a unique parameter  $\phi$ .

### III. DATA ANALYSIS AND RESULTS

#### A. Time series

With the framework presented in the previous section, time-dependent measurements of different experiments have been converted into comparable time series of modulation potentials  $\phi(t)$ . An important dataset consists in direct CR measurements on monthly basis from spacecraft. It includes helium flux measurements from the MED instrument onboard the IMP-8 satellite (from 1973 to 1997), and carbon flux measurements from the CRIS experiment onboard ACE (from 1997 to 2020). The ACE/CRIS data cover seven energy intervals between 59 to 200 MeV/n of kinetic energy per nucleon, corresponding to 0.7 to 1.3 GV of carbon rigidity. The IMP-8/MED data covers the range 140 - 380 MeV/n, corresponding to about 1 - 1.6 GV of helium rigidity. To combine the two datasets, we use the highest energy interval of the ACE time series. We obtain a unique time series of CR flux measurements covering 48 years with a mean rigidity value  $R \cong 1.25$  GV. For each month, the data are fitted with the modulated flux of Eq. 1 where the parameter  $\phi$  is left as free parameter. The minimizing function is given by:

$$\chi_i^2(\phi) = \sum_k \left[ J_i^{\text{mod}}(E_k, \phi) - \hat{J}_i(E_k) \right]^2 \sigma_{i,k}^{-2}, \quad (7)$$

where  $\hat{J}_i(E_k)$  is the  $i$ -th measurement of CR flux, along with its uncertainty  $\sigma_{i,k}$ . In spacecraft data, statistical uncertainties are of the order of  $\sim 5$ -10%, while systematic uncertainties are 2-3%. The flux  $J_i^{\text{mod}}$  is FF-modulated using the input LIS of that species and calculated at the energies  $E_k$  of the data. In practice, the two series from ACE and IMP-8 cover distinct epochs, so that we end up with a unique ACE+IMP-8 series  $\phi_i = \phi(t_i)$ . Similar time series have been derived using counting rates from NM detectors. In this work, we have considered six stations: Oulu, Kiel, Newark, Moscow, Jungfraujoch, and Rome. The main properties of these NM stations are summarized in Table I. The considered stations have a large time span, covering at least 55 years of data, and different rigidity cutoff ranging from 0.8 to 6.7 GV. The rigidity cutoff of a NM station depends on its location in the local geomagnetic field. It is calculated as the vertical Stoermer cutoff [58]. The data of each station consist in monthly averaged rates. All rates are corrected for barometric pressure and detection efficiency [15]. For each dataset  $d$ , the corresponding time series of  $\phi^d$  has been determined with a minimization procedure. Given the measured rate for the  $i$ -th month  $\hat{\mathcal{R}}_{d,i}$ , the minimizing function is:

$$\chi_{d,i}^2 = \left[ \frac{\mathcal{R}_i^d(\phi) - \hat{\mathcal{R}}_i^d}{\sigma_i^d} \right]^2, \quad (8)$$

where  $\hat{\mathcal{R}}_i^d(\phi)$  is calculated in Eq. 3 and its dependence on  $\phi$  is contained in  $J_i^d$ , see Eq. 1. The  $\sigma_i^d$  factors are the

total uncertainties in the NM rates, that are of the order of  $\sim 8$ -10% [49]. From the NM rates, we obtain seven time series  $\phi_d(t_i)$  over the same time period that can be compared with each other. The measured NM rates are shown in the top panel of Fig. 2. The corresponding time series of modulation potential are shown in the bottom panel. All time series agree fairly well within the uncertainties. Little discrepancies or glitches can be noted for a few stations. They can be related to unaccounted inefficiencies, dead time, or other sources for unstable behavior [56]. Nonetheless, the NMs operated with high stability, overall, during the long observation period of this work.

As a proxy of solar activity, we consider the SSN data provided on monthly basis (calendar months) [4]. Thus, we define a continuous function  $S(t)$  that interpolates the 13-month smoothed SSN series. In the left panel of Fig. 3, the time evolution of the monthly (blue) and smoothed (orange) SSN is shown for five solar cycles. The SSN data are compared with the reconstruction of the CR modulation potential  $\phi$ . The modulation parameter is shown in the right panel for two datasets: spacecraft data on CR fluxes from MED/IMP-8 and CRIS/ACE (red line), and NM rates from the Rome station (green area). In the figure, the starlike structure of the graphs reflects the quasiperiodicity of the solar cycle. The  $\phi$  time series from spacecraft data shows a similar structure of those obtained with NM rates. Some little discrepancies are observed during solar maxima. They can be ascribed to known features of the FF model in the low-energy region [46, 60]. Moreover, the two plots show a similar starlike structure. This reflects the known anticorrelation between SSN and CR flux. However, here we observe a *positive* correlation because we consider the modulation potential in place of the CR flux.

#### B. Time lag analysis

From the existence of a time lag  $\tau$  between solar activity and CR flux modulation, we expect that the parameter  $\phi$  calculated at epoch  $t$  should be maximally correlated with the SSN observed at a previous epoch  $t - \tau$ . This can be noticed from the graphs in Fig. 3. Here the *modulation star* (right) shows a small tilt toward counterclockwise direction in comparison with the *sunspot star* (left). Note that a rigid tilt would reflect and unique and constant time shift. In the present work, we investigate whether and how the modulation lag *evolves* over the solar cycle. To determine the lag  $\tau_d$  between the  $d$ th time series  $\phi^d$  and the SSN, we use a criterion based on the maximum correlation. For a set of observations on CR fluxes and SSN in a given time interval, our best estimate of the lag is the parameter  $\hat{\tau}_d$  for which the degree of correlation between  $\phi^d(t)$  and  $S(t - \tau_d)$  is maximum. Note that as proxy for solar activity we use the smoothed SSN series. This allows us to work with a continuous function  $S(t - \tau)$ . To evaluate the degree

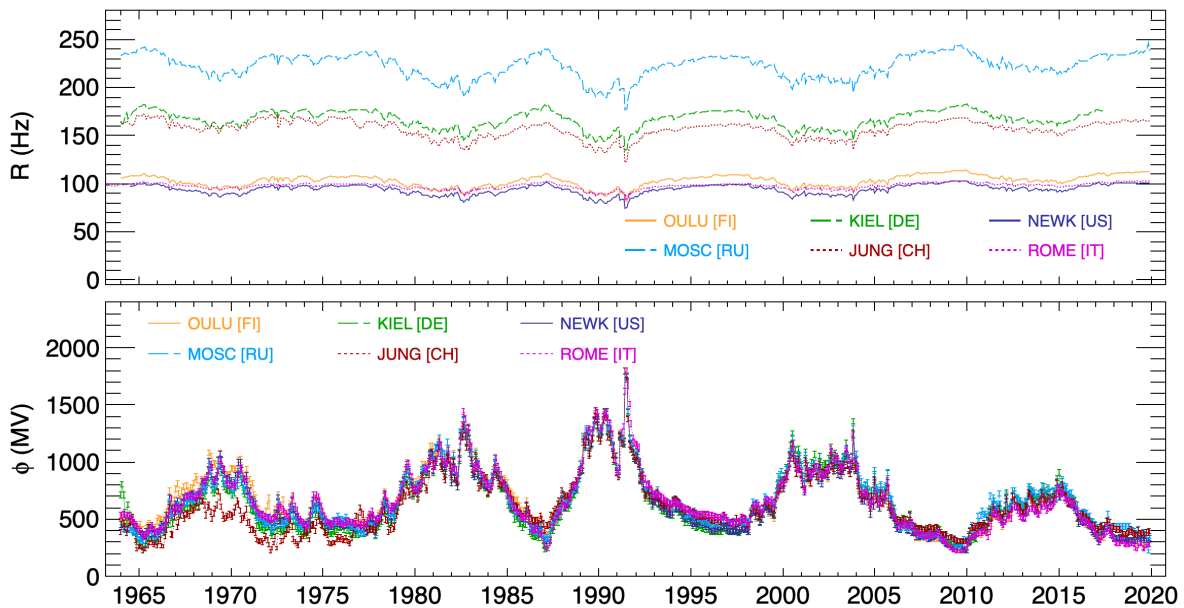


FIG. 2. Temporal dependence of NM counting rates  $\mathcal{R}^d(t)$  for six detector stations (top) and the corresponding reconstruction of the modulation potential  $\phi^d(t)$  (bottom) on monthly basis from 1965 to 2020.

NM station	NEWK	OULU	KIEL	JUNG	MOSC	ROME
Detector type	6-NM64	9-NM64	18-NM64	3-NM64	24-NM64	20-NM64
Location	Newark, US	Oulu, FI	Kiel, DE	Jungfrauoch, CH	Moscow, RU	Rome, IT
Coordinates	39.68 N 75.75 W	65.05 N, 25.47 E	54.32 N, 10.12 E	46.55 N, 7.98 E	55.47 N, 37.32 E	41.86 N, 12.47 E
Altitude	50 m	15 m	54 m	3570 m	200 m	0 m
Cutoff	2400 MV	810 MV	2360 MV	4500 MV	2430 MV	6700 MV

TABLE I. Main characteristics of the NM stations used in this work (from <http://www.nmdb.eu> [15]).

Parameters	IMP-8 + ACE	OULU	KIEL	NEWK	MOSC	JUNG	ROME
$\tau_M$ (months)	$9.82 \pm 0.42$	$7.76 \pm 0.40$	$7.37 \pm 0.45$	$7.36 \pm 0.38$	$7.56 \pm 0.41$	$7.99 \pm 0.52$	$8.33 \pm 0.41$
$\tau_A$ (months)	$4.87 \pm 0.55$	$5.22 \pm 0.55$	$4.99 \pm 0.60$	$5.00 \pm 0.52$	$5.31 \pm 0.56$	$5.64 \pm 0.71$	$4.76 \pm 0.56$
$T_0$ (years)	$21.44 \pm 0.73$	$21.20 \pm 0.58$	$22.22 \pm 0.85$	$21.04 \pm 0.58$	$21.56 \pm 0.63$	$20.99 \pm 0.75$	$21.63 \pm 0.67$
$t_P$ (years)	$2.25 \pm 0.51$	$1.50 \pm 0.44$	$3.09 \pm 0.64$	$1.42 \pm 0.43$	$1.61 \pm 0.44$	$1.32 \pm 0.55$	$2.05 \pm 0.52$

TABLE II. Summary of the fit results on individual datasets with the parameters of Eq. 9.

of correlation with a given lag  $\tau$ , we make use of the Spearman's rank-order correlation coefficient as default,  $\rho_S^d = \rho_S^d(\tau)$ . The procedure is based on a running window technique and it is outlined as follows. First, we define a time grid  $\{t_k\}_{k=1}^N$  of  $N$  equidistant epochs (with constant pitch  $p_t \equiv t_{k+1} - t_k$ ) over the total observation period. For each epoch  $t_k$ , we build a  $\delta_t$ -sized window  $[t_k - \delta_t, t_k + \delta_t]$ . Thus, we analyze the  $\phi$ -SSN correlation inside that window. More precisely, for every dataset  $d$  we compute the correlation coefficient  $\rho_S^d(\tau)$  between two sets of data: all monthly evaluations of  $\phi^d(t)$  where  $t$  lies in the considered window, and their corresponding SSN values  $S(t - \tau)$  evaluated at the time  $t - \tau$ . At this point, to estimate the lag, we repeat the procedure multiple times by varying the lag parameter. In prac-

tice we make a tight scan between  $\tau = -6$  and  $\tau = 24$  months. For all the considered epochs, the resulting function  $\rho_S^d(\tau)$  appears to be remarkably Gaussian-shaped around a maximum value. The maximum  $\hat{\tau}_d$  is taken as the best estimate of the lag in the considered epoch  $t$ , for the dataset  $d$ . Typical values are  $\hat{\tau}_d \sim 3$ -12 months. The advantage of the Spearman's coefficient lies on its independence on any functional relationship between the two variables. Along with Spearman, other correlation coefficients have been tested. The dependence of various correlation coefficients on the lag parameter  $\tau$  are shown in Fig. 4 for the Oulu dataset. The following coefficients are shown in the figure: the Pearson's product-moment correlation  $\rho_P^d$ , which is a measure of the *linear* correlation between  $\phi^d$  and SSN; the Matisse  $\rho_M^d$ , which

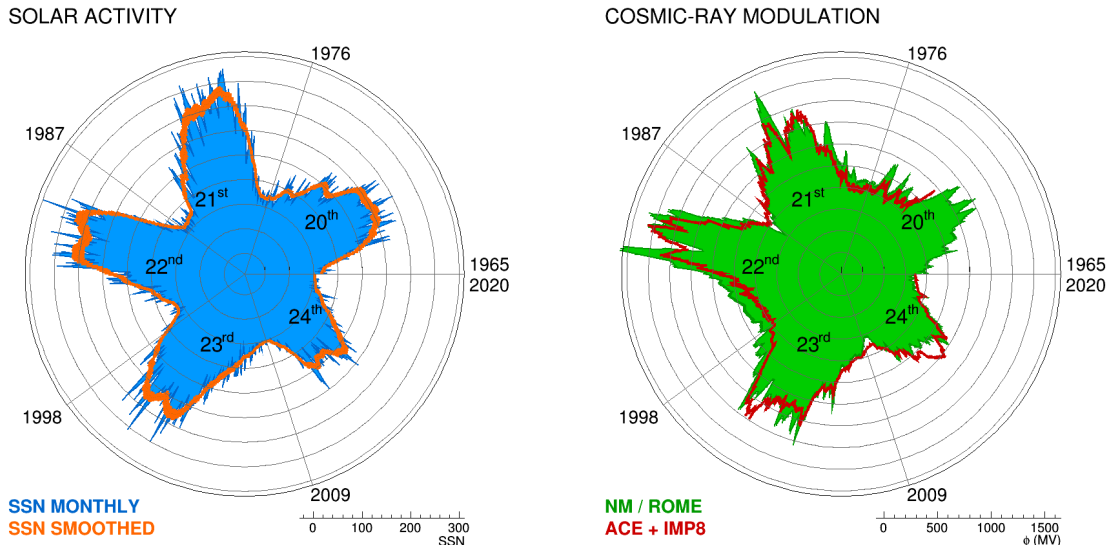


FIG. 3. Temporal evolution of the monthly SSN (blue) and its smoothed value  $S(t)$  (orange) since 1965 to 2020. Right: evolution of the monthly modulation potential  $\phi$  reconstructed using NM data from the SVIRCO station in Rome, Italy (green) and using direct CR measurements in space made from IMP-8 (1973-1997) and ACE (1997-2020).

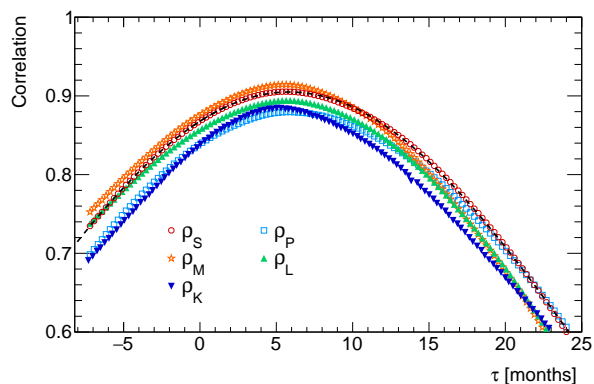


FIG. 4. Correlation coefficients evaluated as function of the assumed time-lag  $\tau$  between SSN and CR flux. The graphs have been obtained with the Oulu NM dataset between 1986 and 1988. A Gaussian fit is shown for the curve obtained with the Spearman coefficient.

measures the linear correlation between  $\phi^d$  and the logarithm of SSN, as discussed in Tomassetti et al. [25]; the  $\rho_L^d$  *log-log* coefficient which measures the Pearson correlation of both logarithms of  $\phi$  and SSN; the Kendall rank correlation coefficient  $\rho_K^d$ ; finally, the Spearman's correlation coefficient  $\rho_S(\tau)$  which is shown together with a Gaussian fit. From Fig. 4, it can be seen that all the correlation methods agree with a maximum correlation at  $\hat{\tau} \approx 5 - 6$  months. The procedure is applied to the whole observation periods and for all the time series. For each dataset  $d$ , we end up with a time series of lag values  $\tau^d$ . The results are found to be robust against the use of multiple datasets and different correlation coefficients. They are also stable against the SSN smoothing

parameters, the  $\delta_t$  and  $p_t$  parameters the time window. The impact of theoretical uncertainties in the LIS models, uncertainties on the smoothed SSN variance, in the correlation coefficients, in the determination of  $\hat{\tau}$  was assessed. The reconstructed evolution of the lag is shown in Fig. 5. Here results are shown for CR data from space (left) and from the Rome NM station (right), over the last five solar cycles. It can be seen that both time series show a remarkable periodicity. In the figure, the data are fitted with a sinusoidal function (dashed line):

$$\tau^d(t) = \tau_M^d + \tau_A^d \cdot \cos \left[ \frac{2\pi}{T_0^d} (t - t_P^d) \right], \quad (9)$$

where  $\tau_A$  is the maximum amplitude of its variation,  $T_0$  is the oscillation period, and  $t_P$  is the phase. The function oscillates around  $\tau_M^d$ , its average value. Both datasets of Fig. 5 give a best-fit period  $T_0 = 21.5 \pm 0.8$  years. The reconstructed lag from all the free parameters of Eq. 9 are summarized in Table II. It can be seen that the different NM stations lead to consistent results. We also note that some points seem to deviate from the periodical model, in particular around the minima/maxima. Here the behavior looks a bit sharper than that of a simple sinusoidal. In our opinion, some of these features may be related to irregularities in the solar cycle, while the overall trend may be different from a perfect periodical and sinusoidal. Clearly, the sinusoidal model is a simplification of the actual trend, which could probably be described by better models. Nonetheless, it captures well the 22-year periodicity of the modulation lag. A further evidence for this periodicity is provided in Fig. 7. Here the Fourier transform of the modulation lag is plotted for all time-series (NM and spacecraft data). The fig-

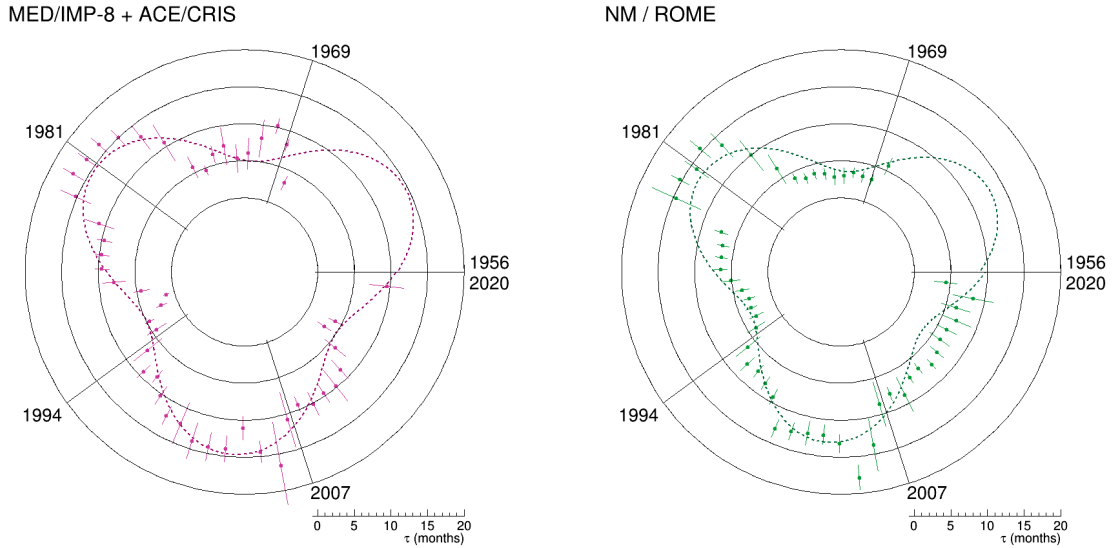


FIG. 5. Temporal evolution of the CR modulation lag reconstructed on yearly basis over five solar cycles. The two reconstructions are done using CR data from ACE/IMP-8 (left) and from the NM station in Rome (right). The dashed lines are a sinusoidal fit of Eq. 9, showing a best-fit period  $T \approx 22$  years.

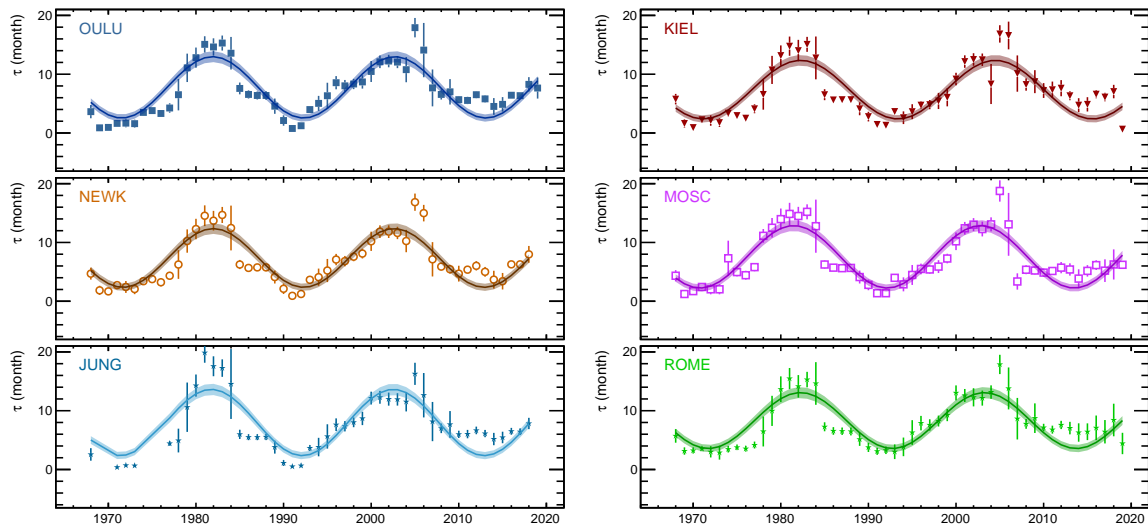


FIG. 6. Temporal evolution of the CR modulation lag reconstructed on yearly basis over five solar cycles. The reconstructions are obtained from NM rates of the six stations in Table I. The solid lines show a fit to the data with Eq. 9, along with their with 68% CL uncertainty bands.

ure shows the 22-year periodicity peak as a dominant periodicity of the time-lag variation. As an independent cross-check, we applied a different fit strategy. The parameters of Eq. 9 were determined by maximizing directly the correlation between  $\phi^d(t)$  and  $S(t - \tau^d(t))$ . In this approach, the smoothed SSN function  $S$  depends on the  $\tau^d(t)$  function, which is expressed as analytical function of the parameters  $\Theta \equiv \{\tau_M, \tau_A, T_0, t_P\}$ , from Eq. 9. Thus, for any set of lag parameters  $\Theta$ , one can compute the correlation coefficient  $\rho_S^d = \rho_S^d(\Theta)$ . We define the minimizing function as  $\tilde{\chi}^d(\Theta) \equiv 1 - |\rho_S^d(\Theta)|^2$ . The best-fit estimate of the lag parameters was obtained

by the minimization of this function. For all minimizations, we use C++ routines of MINUIT implemented in the ROOT package. This procedure has the advantage of providing directly the lag parameters. There is no need of splitting the time series into subintervals and to reconstruct the whole lag evolution. On the other hand, the results are no longer model independent. They rely on the assumed functional dependence for the evolution of the lag (*i.e.*, Eq. 9). Nonetheless the two independent cross-checks gave consistent results.

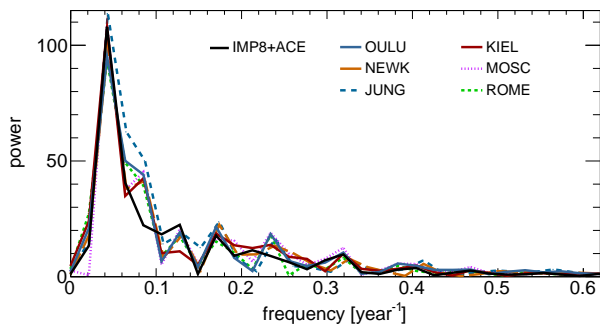


FIG. 7. Fast Fourier transform of the evolution of the modulation lag calculated using CR data from space (ACE+IMP8 combined) and from NM rates of several stations. All time series agree with the presence of a dominant frequency of  $1/(22 \text{ year})$ .

### C. Rigidity dependence

The use of several datasets allows us to inspect the energy or rigidity dependence of the parameters. In the following we make use of rigidity  $R$ . The time series from spacecraft data is evaluated at  $R = 1.25 \text{ GV}$ . The other time series from NM are unresolved on rigidity. Nonetheless, from Eq. 3, one can compute the average rigidity of CRs producing the NM rates, which is of the order of dozens GV. We then define the *mean rigidity*  $\langle R^d \rangle$ , for the  $d$ -th dataset, as the time-averaged expectation value of  $R$ . The average is calculated on CR energy spectrum that produces the observed rates. We write:

$$\langle R^d \rangle \equiv \frac{1}{N^d} \sum_j \int_T dt \int_0^\infty R_j \mathcal{H}_j^d \mathcal{Y}_j^d J_j dE, \quad (10)$$

where all the quantities in the integrand function, including  $R_j$ , are expressed as function of kinetic energy per nucleon  $E$ . The  $N^d$  factor represents the normalization and it is given by:

$$N^d \equiv \sum_j \int_T dt \int_0^\infty \mathcal{H}_j^d \mathcal{Y}_j^d J_j dE. \quad (11)$$

Thus, the calculation of  $\langle R^d \rangle$  involves the CR spectra, the NM yield function, the transmission function. In particular, it depends on the geomagnetic rigidity cutoff  $R_C^d$ , which varies from NM to NM. From Table I, the cutoff range from 0.8 GV (Oulu) to 6.7 GV (Rome). Using NMs at different cutoff, one may study the rigidity dependence of NM rates [16]. In fact the integral in Eq. 10 is suppressed at  $R \lesssim R_C$ , thus  $\langle R^d \rangle$  increases with  $R_C$ . However, this dependence is mitigated by the NM yield function  $Y^d(R)$ , which decreases rapidly with decreasing rigidity. As a result, we found that all NMs give similar values for the mean rigidity, between  $\sim 25$  and  $35 \text{ GV}$ . In Fig. 8, the best-fit parameters of Eq. 9 are plotted as function of  $\langle R^d \rangle$ . From the figure, it can be seen that all NM data group together at  $\langle R^d \rangle \sim 30 \text{ GV}$ . As noted in Ref. [22], from NM data alone it is difficult to determine

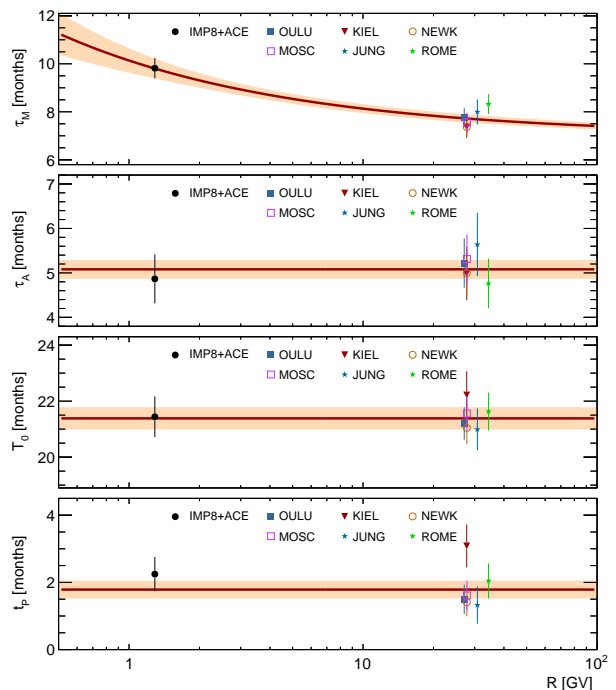


FIG. 8. Best-fit values of the lag parameters of Eq. 9 for all time-series plotted against the mean rigidity  $\langle R \rangle$ . The solid lines show the global fit according to Eq. 12, along with the 68% CL bands.

any rigidity dependence. Noticeably, all the datasets agree with a  $T_0$  parameter fairly consistent with the period of a magnetic polarity cycle, 22 years. Similarly, phase and amplitude give consistent results, showing no indications for rigidity dependence. In the figure, these parameters are fitted with constant functions. On the other hand, the average lag value  $\tau_M$  shows a remarkable *decrease* with increasing CR rigidity. From the fits, the low- $R$  data give an average lag  $\tau_M$  of nearly ten months, while all NM data agree with a mean lag of about eight months. To fit its rigidity dependence, we used a function of the type  $\tau_M(R) = \tau_{\text{Min}}^0 + \tau_M^0 (R/\text{GV})^{-\alpha}$ , *i.e.*, a power-law in rigidity  $R$  with index  $\alpha$  plus a constant offset  $\tau_{\text{Min}}^0$ . As we discuss in the next section, the choice of the power-law function is based on considerations on the rigidity dependence of the CR diffusion timescale. The constant offset must be set to keep  $\tau \geq 0$  in the high- $R$  limit.

### D. A global formula for the modulation lag

Based on the considerations made in the previous paragraph, we end up with the following formula:

$$\tau = \tau_{\text{Min}}^0 + \tau_M^0 \left( \frac{R}{\text{GV}} \right)^{-\alpha} + \hat{q} \tau_A \cos \left[ \frac{2\pi}{T_0} (t - t_P) \right] \quad (12)$$

The equation describes the rigidity and temporal evolution of the modulation lag over the solar cycle. The



best-fit parameter values are the following:  $\tau_M^0 = 3.1 \pm 0.5$  months,  $\alpha = 0.5 \pm 0.09$ ,  $T_0 = 21.4 \pm 0.5$  years, and  $t_P = 1.8 \pm 0.2$  months. The equation is shown in Fig. 8 (thick red line) along with its “one  $\sigma$ ” uncertainty (yellow band) associated with the fit. In Eq. 12, the factor  $\hat{q} \equiv q/|q|$  is the charge sign of the CR particles. The analysis presented here is based on positively charged particles, so that  $\hat{q} = 1$ . The charge-sign dependence of the lag is linked to the dependence of the modulation equations on the  $\hat{q} \cdot A$  product between CR charge-sign and solar magnetic polarity. This dependence could be tested directly using time-resolved data on cosmic antiparticles such as, in particular, AMS measurements on CR antiprotons. The formula can also be expressed in terms of cycle fraction  $x \equiv t/T_0$ , in place of the time variable, which makes it useful to be applied or tested to other/future solar cycles. The equation is valid only for CR located near-Earth (at helioradius  $r_0 = 1$  AU). Other regions of the heliosphere may have different lag parameters. In spite of its simplicity, this equation represents a generalization of the empirical delay factors used in many time-dependent modulation models [25, 32–34], which are often kept as constant. The lag evolution over the different phases of the solar cycle is also illustrated in Fig. 9 and discussed in the following.

## IV. DISCUSSION

### A. Interpretation of the results

The modulation lag is often interpreted in terms of timescales of the changing conditions of the heliosphere. The process is regulated by the propagation speed  $V$  of the solar wind, which fills a modulation region of size  $L \sim 100$  AU. The naive estimate suggests a modulation lag of the order of one year,  $\tau \sim L/V$ . However, the present study suggests a more complex physical picture where also drift, latitudinal dependence of the wind, and CR diffusion play an active role in the formation of the lag. A similar picture is also emerging from recent works [24, 31, 61], as we discuss in the next paragraph. Because of gradient or curvature drifts across the interplanetary magnetic field, CRs are guided to follow preferential trajectories. Hence, near-Earth observations of CRs probe only selected regions of the heliosphere. The drift speed of CRs, however, depend on the product  $\hat{q}\hat{A}$ . During  $\hat{A}^+$  epochs, cosmic protons reach the inner heliosphere through high-latitude regions. During  $\hat{A}^-$  epochs, they gather near the equatorial plane and across the heliospheric current sheet. This phenomenon is coupled with the colatitudinal dependence of the solar wind. The wind speed  $V(\theta)$  ranges from  $\sim 400$  km s $^{-1}$  near equators ( $\theta \sim 90^\circ$ , slow wind region) to  $\gtrsim 800$  km s $^{-1}$  in the polar regions ( $\theta \sim 0^\circ, 180^\circ$ , fast wind region) [1]. As a consequence, we expect larger lags when analyzing CR data in  $\hat{q}\hat{A} < 0$  conditions, as we are probing the slow-wind region. In contrast, shorter lags are expected from data

of  $\hat{q}\hat{A} > 0$ , that probe the fast-wind regions of the heliosphere. Moreover, we expect that matter and antimatter particles interchange their role with the change of polarity. The propagation of CR protons (or positrons) under  $\hat{A}^+$  periods should be similar to that of CR antiprotons (or electrons) during  $\hat{A}^-$  periods and viceversa. This circumstance is expressed by the factor  $\hat{q}$  in Eq. 12 and could be resolutely tested using time-resolved data on CR antimatter. The connection between the modulation lag and the 22-year polarity cycle is also illustrated in Fig. 9. In the figure, along with the solar cycles, the  $\hat{A}^+/\hat{A}^-$  magnetic polarities are shown.

In addition, the observed rigidity dependence suggests that the propagation times of CRs in the heliosphere play a crucial role in the formation of the lag. Here we refer to the time spent by CRs in the heliosphere before reaching Earth. Their propagation time is dominated by parallel diffusion with a coefficient of the type  $K \propto R^\alpha$ , where the index  $\alpha$  is linked to the spectrum of magnetic turbulence [54]. Hence, the CR propagation time must decrease with rigidity as  $T_{\text{diff}} \sim L^2/3K(R) \propto R^{-\alpha}$ . As a result, low- $R$  particles bring more “delayed” information in comparison with high- $R$  particles. In particular, the diffusion time of 1 GV particles is of the order of one month [62, 63]. Such a rigidity-dependent lag, however, adds up to a rigidity-independent lag which is of the order of 6-8 months. After considering both terms, we end up with the final form of Eq. 12. Intriguingly, this result may offer a new way to measure the rigidity dependence of CR diffusion in heliosphere. The parameter  $\alpha$  of the present work agrees with other analysis based on CR propagation models [54],

### B. Comparison with other works

The study of the time lag in the long-term CR modulation was conducted in a number of recent works. Different techniques of data processing or analysis approaches were used [22, 23, 61]. Several studies on the long-term CR modulation have pointed to an odd/even effect for the lag. The lag observed during odd solar cycles appears to be longer than that in even ones. These observations suggest the association of this feature with charge-sign dependent drift [17, 64]. In this work, we determined the temporal evolution of the modulation lag over five solar cycles. This shows its quasiperiodical behavior in connection with the 22-year solar cycle of magnetic polarity. The role of drift is essential for the interpretation given in Sec. IV A. Two interesting papers appeared while this work was in preparation [24, 31]. In Koldobskiy et al. [24], the variability of the CR modulation lag is investigated by means of a time-frequency wavelet analysis. A complete compilation of the past results is also presented, showing the modulation lags reported at different epochs/cycles. Their results agree well with ours. In Wang et al. [31], it is suggested that the time lag between CR flux and SSN originates already in the open magnetic flux on the Sun. The lag between SSN and the genera-

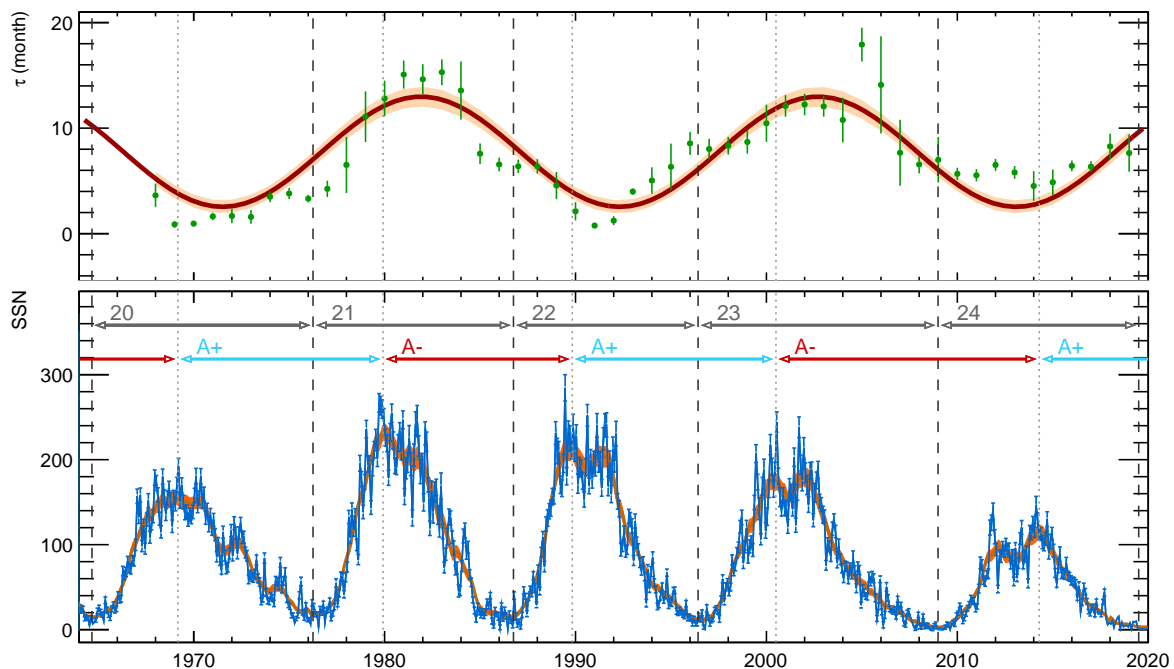


FIG. 9. Temporal evolution of the modulation lag determined using NM data from the Oulu station (top), in close comparison with the evolution of the SSN (bottom) over the last five solar cycles. The solid line shows the sinusoidal fit of Eq. 9 and its associated uncertainties. The dashed and dotted lines indicate solar cycle minima and maxima, respectively, defining cycle numbers and their magnetic polarities.

tion of the open magnetic flux was also analyzed. The authors found a cycle-dependent lag that might explain the odd/even effect. They also note that the role of CR transport should make a contribution. In Sec. III C and Sec. IV A, we also came to the conclusion that the lag originates from different contributions. However, the delayed open flux scenario was not considered in our work. In Sec. III C, to determine the rigidity dependence of the lag, we have defined the mean rigidity  $\langle R \rangle$  of CRs that forms the NM rates. The notion of the effective CR rigidity (or energy)  $R_{\text{eff}}$  for NMs is discussed in many works [65–68]. In Gil et al. [66], it is defined as the CR rigidity at which protons have the same relative variability as the counting rate of the detector. In Alanko et al. [65],  $R_{\text{eff}}$  is defined such that the NM rate is proportional to the flux of all CRs with rigidity  $R$  above this value. In this paper, our definition of  $\langle R \rangle$  is aimed at capturing the *average* rigidity value of the primary CRs that produce the NM signal. Comparing the two definitions, one expects that  $\langle R \rangle$  is some factor larger than  $R_{\text{eff}}$ . The rigidity dependence of the modulation lag is investigated first in Nymmik [16], where the simple cut-off value  $R_C$  was used as reference rigidity. We find, in agreement with this work, the general trend that odd solar cycles show longer lags than even cycles. We did not find, however, any odd/even effect in the rigidity dependence of the lag. Moreover, in agreement with Ross & Chaplin [22], we found that the NM data alone do not lead to a clear determination of rigidity dependence. It is also interesting to compare our work with the results

of Shen et al. [61]. In their work, the energy dependence of the lag was derived using only spacecraft data. Using IMP-8 proton data between 1980 and 1999, they found a decrease for  $\tau(E)$  between about 50 MeV and nearly 400 MeV of kinetic energy. These energies fall just below the range considered in our work. In the highest region, corresponding to about 1 GV of CR proton rigidity, they reported a modulation lag of  $\tau \sim 10$  months for the  $\hat{A}^-$  dataset (epoch 1980-1989) and  $\tau \sim 6$  months for the  $\hat{A}^+$  dataset (epoch 1991-1999). Their results are in agreement with our findings for the same considered periods. However their analysis is only limited to the descending phases of the solar cycle. In Shen et al. [61], the rigidity dependence of the modulation lag is described by a simple power-law function. Their interpretation of such a dependence is in full agreement with ours. However, they derived two distinct slopes for the two datasets of opposite magnetic polarity, suggesting that the lag decreases more rapidly during  $\hat{A}^+$  epochs. The authors argue that a difference in the two slopes may be caused by different rates of CR energy losses in the two magnetic polarities. Although such an interpretation appears reasonable to us, it should also be noted that the two trends are very similar each other. Within the uncertainties estimated in our analysis, the discrimination of the of the two slopes is not possible. Regarding Eq. 12, a comparison with past works can be done. In models based on the transport equation, the time lag is usually treated as an input parameter  $\tau$  to be determined with the data [34, 37, 38]. In general, many models rely on the simplifying assumption

of a constant lag [25, 33, 36, 37]. In some recent works, the lag parameter is assumed to take different values for odd/even solar cycles, *i.e.*, it is modeled as a 22-year periodic step function [32, 33]. In the BOM model [32, 35], the temporal evolution of the CR flux is calculated within the FF approximation. The time dependence of the modulation parameter  $\Phi(t)$  is calibrated against the SSN using a cycle-dependent delayed relationship. In practice, a two-value lag is used as input parameter, depending on the odd/even cycle number. The same approach is used in other approaches, including fully empirical models [29, 37]. In this respect, our formula can be regarded as a generalization of early attempts to account for the lag in CR modulation.

### C. Further developments

The study of the relationship between CR modulation and solar activity provides the basis for establishing the long-term forecast of the CR radiation levels in the heliosphere. Forecasting CR radiation is an important concern for crewed space travel in future missions [2]. In light of the comparison with other studies, further correlative analyses may be carried out the use of other proxies carrying different information. Examples are indices as the open magnetic flux, the tilt angle of the heliospheric current sheet, the solar irradiance, the flare index. Using these indices, one can in principle allow to assess the different contributions of the modulation lag. Regarding the interpretation, we discussed our results in general terms of large-scale diffusion and drift, but the role of merged interaction regions in the time-dependent CR modulation should be investigated. Another goal is to calculate the precise rigidity dependence of the CR propagation times in the difference phases of the solar cycle. This will be done in a forthcoming work, based on stochastic simulations of CRs in the heliosphere and time-dependent constraints from AMS/PAMELA data [54].

To improve the study of the rigidity dependence of NM rates, one can set up more refined calculations of the transmission function. In this work, variations in the cutoff  $R_C$  were neglected, although in the last five cycles it decreased of nearly 5% in the equatorial regions [59]. However, NM rates remain unsuitable to study the rigidity dependence of the lag, while direct CR data from space would be of help. In the present study, we considered data from ACE and IMP-8 at the GV scale. The observational gap in the  $\sim 1$ -30 GV rigidity region may be fulfilled with the data from new-generation experiments in low-Earth orbit such as AMS, PAMELA and CALET. The AMS experiment has now covered one solar cycle of exposure. In particular, the AMS experiment in the International Space Station can provide measurements of CR antiprotons over about one solar cycle of exposure. With time series of antimatter/matter data, the

charge-sign dependence of the modulation lag can be determined, and the physical interpretation provided here can be resolutely tested.

## V. CONCLUSIONS

In this paper, we have investigated the delayed association between the variability of solar activity and the temporal variation of CR fluxes. Using a large collection of CR flux measurements from spacecraft and counting rates from NMs, we have reported the observation of important features in the solar modulation effect of CRs in the heliosphere. First, we have shown that the modulation lag between SSN and CR flux is subjected to a quasiperiodical behavior which follows the 22-year cycle of Sun's magnetic polarity. Moreover, we have found that the mean value of the modulation lag decreases with the rigidity or energy of the cosmic particles. These features reveal important aspects of the physics of CR modulation phenomenon. We interpreted our findings in terms of the combination of basic processes of charged particle transport: drift of CRs over the large-scale interplanetary magnetic field, convection over the latitudinal-dependent solar wind, and rigidity dependent diffusion in the magnetic irregularities of heliospheric turbulence. Based on this interpretation, we have proposed an effective formula for describing the temporal evolution and the rigidity dependence of the CR modulation lag. Our formula could be used as an effective input in solar modulation models for making predictions of the CR radiation driven by solar activity proxies. Within the physical picture presented here, the observed connection between modulation lag and solar cycle can be considered as a remarkable signature of charge-sign dependent drift in CR transport. The interpretation could be resolutely tested using data on CR antimatter collected from AMS over a full decade of observation.

## VI. ACKNOWLEDGEMENTS

We acknowledge the support of Italian Space Agency (ASI) under Agreement No. ASI-UniPG 2019-2-HH.0. We also acknowledge the project *DRIFT* - “Cosmic antimatter drifting through the solar wind” in the program Fondo Ricerca di Base 2019 of the University of Perugia. In this work, use was made of the *NMDB.eu* real-time database (for NM rates), the *Cosmic-Ray Database* of the Space Science Data Center at ASI (for CR data from AMS and PAMELA), the *OMNIWeb* service of the NASA Space Physics Data Facility (for spacecraft data), and the *SILSO* SSN database of the *Solar Influences Data Analysis Center* at the Royal Observatory of Belgium. We also thank Nikolay Kuznetsov and Elena Popova for support with the digitized IMP-8 data, Ilya Usoskin for sharing the time series of the  $\phi$  parameter.

- [1] M. S. Potgieter, *Solar Modulation of Cosmic Rays*, *Living Rev. Sol. Phys.*, 10, 3 (2013);
- [2] M. Durante, & F. Cucinotta, *Physical basis of radiation protection in space travel*, *Rev. Mod. Phys.* 83, 1245 (2011);
- [3] J. W. Norbury, K. Whitman, K. Lee, T. C. Slaba, F. F. Badavi, *Comparison of space radiation GCR models to recent AMS data*, *Life Sci. Space Res.* 18, 64-71 (2018);
- [4] F. Clette, & L. Lefèvre, *The New Sunspot Number: Assembling All Corrections*, *Sol. Phys.* 291, 2629-2651 (2016); see also <http://www.sidc.be>;
- [5] J. A. Van Allen, *On the modulation of galactic cosmic ray intensity during solar activity cycles 19,20,21,22 and early 23*, *JGR* 27, 2453-2456 (2000);
- [6] I. G. Usoskin, G. A. Bazilevskaya, G. A. Kovaltsov, *Solar modulation parameter for cosmic rays since 1936 reconstructed from ground-based neutron monitors and ionization chambers*, *JGR* 116, A02104 (2011);
- [7] F. B. McDonald, Z. Fujii, B. Heikkila, N. Lal, R. E. McGuire, *The radial distribution of galactic cosmic rays in the heliosphere at solar minimum and solar maximum*, *Proc. 28-th ICRC Conference*, 3965-3968 (2003);
- [8] A. C. Cummings, E. C. Stone, B. C. Heikkila, et al., *Galactic cosmic rays in the local interstellar medium: Voyager 1 observations and model results*, *ApJ* 831, 18 (2016);
- [9] M. Wiedenbeck, A. J. Davis, C. M. S. Cohen, et al., *Time Dependence of Solar Modulation throughout Solar Cycle 23as Inferred from ACE Measurements of Cosmic-Ray Energy Spectra* *Proc. 31<sup>st</sup> ICRC - Lodz*, 0545 (2009);
- [10] P. Kùhl, R. Gómez-Herrero, B. Heber, *Annual Cosmic Ray Spectra from 250 MeV up to 1.6 GeV from 1995 - 2014 Measured with the Electron Proton Helium Instrument onboard SOHO*, *Sol. Phys.* 291, 965-974 (2016);
- [11] O. Adriani, G. C. Barbarino, G. A. Bazilevskaya, et al., *Time dependence of the proton flux measured by PAMELA during the 2006 July - 2009 December solar minimum*, *ApJ* 765, 91 (2013);
- [12] M. Martucci, R. Munini, M. Boezio, et al., *Proton Fluxes Measured by the PAMELA Experiment from the Minimum to the Maximum Solar Activity for Solar Cycle 24*, *ApJ* 854, L2 (2018);
- [13] M. Aguilar, L. Ali Cavazonza, B. Alpat, et al., *Observation of Fine Time Structures in the Cosmic Proton and Helium Fluxes with the Alpha Magnetic Spectrometer on the International Space Station*, *PRL* 121 (2018) 051101;
- [14] M. Aguilar, L. Ali Cavazonza, G. Ambrosi, et al., *The Alpha Magnetic Spectrometer (AMS) on the international space station: Part II — Results from the first seven years*, *Phys. Rept.* 894, 1-116 (2021);
- [15] P. Väisänen, I. G. Usoskin, K. Mursula, *Seven decades of neutron monitors (1951–2019): Overview and evaluation of data sources*, *JGR Space Phys.* 126, e2020JA028941 (2021);
- [16] R. A. Nymmik, *Time lag of galactic cosmic ray modulation: conformity to general regularities and influence on particle energy spectra*, *ASR* 26, 1875 (2000);
- [17] I. G. Usoskin, K. Mursula, H. Kananen, G. A. Kovaltsov *Dependence of cosmic rays on solar activity for odd and even solar cycles*, *ASR* 27, 571 (2001);
- [18] M. Singh, Y. P. Singh, Badruddin, *Solar modulation of galactic cosmic rays during the last five solar cycles* *J. Atm. & Sol. Terr. Phys.* 70, 169-183 (2008);
- [19] R. P. Kane, *Lags and Hysteresis Loops of Cosmic Ray Intensity Versus Sunspot Numbers: Quantitative Estimates for Cycles 19 – 23 and a Preliminary Indication for Cycle 24*, *Sol. Phys.* 289, 2727-2732 (2014);
- [20] O. P. M. Aslam, & Badruddin, *Study of Cosmic-Ray Modulation During the Recent Unusual Minimum and Mini-Maximum of Solar Cycle 24*, *Sol. Phys.* 290, 2333-2353 (2015);
- [21] P. Chowdhury, K. Kudela, Y. J. Moon, *A Study of Heliospheric Modulation and Periodicities of Galactic Cosmic Rays During Cycle 24*, *Sol. Phys.* 291, 581-602 (2016);
- [22] E. Ross, & W. J. Chaplin, *The behaviour of Galactic cosmic-ray intensity during solar activity Cycle 24*, *Sol. Phys.* 294, 8 (2019);
- [23] K. Iskra, M. Siluszyk, M. Alania, W. Wozniak, *Experimental Investigation of the Delay Time in Galactic Cosmic Ray Flux in Different Epochs of Solar Magnetic Cycles: 1959 - 2014*, *Sol. Phys.* 294, 115 (2019);
- [24] S. A. Koldobskiy, R. Kähkönen, B. Hofer, N. A. Krivova, G. A. Kovaltsov, I. G. Usoskin, *Time Lag Between Cosmic-Ray and Solar Variability: Sunspot Numbers and Open Solar Magnetic Flux*, *Sol. Phys.* 297, 38 (2022);
- [25] N. Tomassetti, M. Orcinha, F. Barao, B. Bertucci, *Evidence for a Time Lag in Solar Modulation of Galactic Cosmic Rays*, *ApJ Lett.* 849, 32 (2017);
- [26] V. K. Mishra, & A. P. Mishra, *Long-Term Modulation of Cosmic-Ray Intensity and Correlation Analysis Using Solar and Heliospheric Parameters*, *Sol. Phys.* 293, 141 (2018);
- [27] K. Nagashima, & I. Morishita, *Long term modulation of cosmic rays and inferable electromagnetic state in solar modulating region* *Plan. & Space Sci.* 28, 177-194 (1980);
- [28] J. Xanthakis, H. Mavromichalaki, B. Petropoulos, *Cosmic-ray intensity related to solar and terrestrial activity indices in solar cycle No. 20*, *Astrophys. Space Sci.* 74, 303-317 (1981);
- [29] H. Mavromichalaki, & B. Petropoulos, *Time-lag of cosmic-ray intensity*, *Astrophys. Space Sci.* 106, 61-71
- [30] I. V. Dorman, & L. I. Dorman, *Solar Wind Properties Obtained from the Study of the 1-Year Cosmic-Ray Cycle, I*, *JGR* 72, 1513 (1967);
- [31] Y. Wang, J. Guo, G. Li, E. Roussos, J. Zhao, *Cosmic Ray Intensity Variation Lags Sunspot number: Implications of Late Opening of Solar Magnetic Field* [arXiv:2201.01908](https://arxiv.org/abs/2201.01908) (2022);
- [32] T. C. Slaba, & K. Whitman, *The Badhwar-O'Neill 2020 GCR Model*, *Space Weather* 18, e2020SW002456 (2020);
- [33] N. V. Kuznetsov, H. Popova, M. I. Panasyuk, *Empirical model of long-time variations of galactic cosmic ray particle fluxes*, *JGR Space Phys.* 122, 1463–1472 (2017);
- [34] D. Matthia, T. Berger, A. I. Mrigakshi, G. Reitz, *A ready-to-use galactic cosmic ray model*, *ASR* 51, 329-338 (2013);
- [35] P. M. O'Neill, *Badhwar O'Neill 2010 galactic cosmic ray flux model—Revised*, *IEEE Trans. Nucl. Sci.* 57, 3148-3153 (2010);
- [36] J. H. Adams; A. F. Barghouty; M. H. Mendenhall, et al., *CRÈME: The 2011 Revision of the Cosmic Ray Effects*

- on Micro-Electronics Code, *IEEE Trans. Nucl. Sci.* 59(6) 3141 (2011); A. J. Tylka, J. H. Adams Jr., P. R. Boberg, et al., *CREME96: A Revision of the Cosmic Ray Effects on Micro-Electronics Code*, *IEEE Trans. Nucl. Sci.* 44, no. 6, pp. 2150-2160 (1997);
- [37] L. L. Zhao & G. Qin, *An observation-based GCR model of heavy nuclei: Measurements from CRIS onboard ACE spacecraft*, *JGR Space Phys.* 118, 1837-1848 (2013);
- [38] C. R. Zhu, Q. Yuan, D. M. Wei, *Studies on cosmic ray nuclei with Voyager, ACE and AMS-02: I. local interstellar spectra and solar modulation*, *ApJ* 863 119 (2018);
- [39] N. Tomassetti, F. Barao, B. Bertucci, J. L. Figueiredo, J. B. Lousada, M. Orcinha, *Testing Diffusion of Cosmic Rays in the Heliosphere with Proton and Helium Data from AMS*, *PRL* 121, 251104 (2018);
- [40] N. Tomassetti, F. Barao, B. Bertucci, E. Fiandrini, M. Orcinha, *Numerical modeling of cosmic-ray transport in the heliosphere and interpretation of the proton-to-helium ratio in Solar Cycle 24*, *Adv. Space Res.* 64, 2477-2489 (2019);
- [41] N. Tomassetti, *Cosmic-ray protons, nuclei, electrons, and antiparticles under a two-halo scenario of diffusive propagation*, *PRD* 92, 081301(R) (2015);
- [42] J. Feng, N. Tomassetti, A. Oliva, *Bayesian analysis of spatial-dependent cosmic-ray propagation: Astrophysical background of antiprotons and positrons*, *PRD* 94, 123007 (2016);
- [43] M. Aguilar, D. Aisa, B. Alpat, et al., *Precision Measurement of the Proton Flux in Primary Cosmic Rays from Rigidity 1 GV to 1.8 TV with the Alpha Magnetic Spectrometer on the International Space Station*, *PRL* 114, 171103 (2015);
- [44] M. Aguilar, D. Aisa, B. Alpat, et al., *Precision Measurement of the Helium Flux in Primary Cosmic Rays of Rigidities 1.9 GV to 3 TV with the Alpha Magnetic Spectrometer on the International Space Station*, *PRL* 115, 211101 (2015);
- [45] M. Aguilar, L. Ali Cavansonza, G. Ambrosi, et al., *Precision Measurement of the Boron to Carbon Flux Ratio in Cosmic Rays from 1.9 GV to 2.6 TV with the Alpha Magnetic Spectrometer on the International Space Station*, *PRL* 117, 231102 (2016);
- [46] N. Tomassetti, *Solar and nuclear physics uncertainties in cosmic-ray propagation*, *PRD* 96, 103005 (2017);
- [47] L. J. Gleeson, & W. I. Axford, *Solar Modulation of Galactic Cosmic Rays*, *ApJ* 154, 1011 (1968);
- [48] R. A. Caballero-Lopez, & H. Moraal, *Limitations of the force field equation to describe cosmic ray modulation*, *JGR* 109, A011101 (2004);
- [49] D. Maurin, A. Cheminet, L. Derome, A. Ghelfi, G. Hubert, *Neutron monitors and muon detectors for solar modulation studies: Interstellar flux, yield function, and assessment of critical parameters in count rate calculations*, (*ASR* 55, 363-389 2015);
- [50] N. Tomassetti, *Testing universality of cosmic-ray acceleration with proton/helium data from AMS and Voyager-1*, *ASR* 60, 815 (2017);
- [51] M. J. Boschini, S. Della Torre, M. Gervasi, et al., *Solution of Heliospheric Propagation: Unveiling the Local Interstellar Spectra of Cosmic-ray Species*, *ApJ* 840, 115, (2017);
- [52] M. J. Boschini, S. Della Torre, M. Gervasi, G. La Vacca, P. G. Rancoita, *The HelMod Model in the Works for Inner and Outer Heliosphere: from AMS to Voyager Probes Observations*, *ASR* 64, 2459-2476 (2019);
- [53] M. S. Potgieter, *The charge-sign dependent effect in the solar modulation of cosmic rays*, *ASR* 53, 1415-1425 (2014);
- [54] E. Fiandrini, N. Tomassetti, B. Bertucci, F. Donnini, M. Graziani, B. Khiali, A. Reina Conde, *Numerical modeling of cosmic rays in the heliosphere: Analysis of proton data from AMS-02 and PAMELA*, *PRD* 104, 023012 (2021);
- [55] A. Gil, I. G. Usoskin, G. A. Kovaltsov, A. L. Mishev, C. Corti, V. Bindi, *Can we properly model the neutron monitor count rate?* *JGR Space Phys.* 120, 7172-7178 (2015);
- [56] A. L. Mishev, S. A. Koldobskiy, G. A. Kovaltsov, A. Gil, I. G. Usoskin, *Updated Neutron-Monitor Yield Function: Bridging Between In Situ and Ground-Based Cosmic Ray Measurements*, *JGR Space Phys.* 125, JA027433 (2020);
- [57] A. Cheminet, G. Hubert, V. Lacoste, D. Maurin, L. Derome, *Cosmic ray solar modulation and Forbush decrease analyses based on atmospheric neutron spectrometry at mountain altitude and GEANT4 simulations of extensive air showers*, *JGR* 118, 7488-7496 (2013);
- [58] D. F. Smart, & M. "P." A. Shea, *A Review of Geomagnetic Cutoff Rigidities for Earth-Orbiting Spacecraft*, *ASR* 36, 2012-2020 (2005);
- [59] E. G. Cordaro, P. Venegas-Aravena, D. Laroze, *Variations of geomagnetic cutoff rigidity in the southern hemisphere close to 70° W (South-Atlantic Anomaly and Antarctic zones) in the period 1975-2010*, *ASR* 63, 2290-2299 (2019);
- [60] J. Gieseler, B. Heber, K. Herbst, *An Empirical Modification of the Force Field Approach to Describe the Modulation of Galactic Cosmic Rays Close to Earth in a Broad Range of Rigidities*, *JGR* 122, 10964 (2017);
- [61] Z. N. Shen, G. Qin, Z. Pingbing, F. Wei, X. Xu, *A Study of Variations of Galactic Cosmic-Ray Intensity Based on a Hybrid Data-processing Method*, *ApJ* 900, 143 (2020);
- [62] J. J. O'Gallagher, *A time-dependent diffusion-convection model for the long-term modulation of cosmic rays*, *ApJ* 197, 495-507 (1975);
- [63] R. D. Strauss, M. S. Potgieter, A. Kopp, I. Büsching, *On the propagation times and energy losses of cosmic rays in the heliosphere*, *JGR* 116, A12105 (2011);
- [64] I. G. Usoskin, G. A. Kovaltsov, H. Kananen, K. Mursula, P. J. Tanskanen, *Phase evolution of solar activity and cosmic-ray variation cycles*, *Sol. Phys.* 170, 447-452 (1997);
- [65] A. Alanko, I. Usoskin, K. Mursula, G. A. Kovaltsov, *Heliospheric modulation strength: effective neutron monitor energy*, *ASR* 32, 615-620 (2003);
- [66] A. Gil, E. Asvestari, G. A. Kovaltsov, I. G. Usoskin, *Heliospheric modulation of galactic cosmic rays: Effective energy of ground-based detectors*, *Proc. 35th Int. Cosmic Ray Conf., PoS(ICRC2017)032* (2018);
- [67] E. Asvestari, A. Gil, G. A. Kovaltsov, I. G. Usoskin, *Neutron Monitors and Cosmogenic Isotopes as Cosmic Ray Energy-Integration Detectors: Effective Yield Functions, Effective Energy, and Its Dependence on the Local Interstellar Spectrum*, *JGR Space Phys.* 122, 9790-9802 (2017);
- [68] S. A. Koldobskiy, G. A. Kovaltsov, I. G. Usoskin, *Effective Rigidity of a Polar Neutron Monitor for Recording Ground-Level Enhancement*, *Sol. Phys.* 293, 110 (2018);